# An Enhanced Method for Instantaneous Angular Speed Accuracy Improvement and Its Application in Variable-Speed Scenarios

Dikang Peng [a], Wei Teng [a], Yibing Liu [a]

❖ [a] *Key Laboratory of Power Station Energy Transfer Conversion and System (North China Electric Power University), Ministry of Education, Beijing 102206, China*

## Highlights:

Uncover amplitude modulation-noise impacts on phase demodulation

Uncover carrier amplitude-noise impacts on phase demodulation

IAS estimate variance can be estimated from signal

Enhanced IAS accuracy improvement method is proposed

Validation on simulated and industrial data via different implementations

## Abstract

Tacholess speed estimation serves as a powerful preprocessing method for condition monitoring of variable-speed machinery in scenarios where speed reference sensors are unavailable. However, for a mono amplitude modulated (AM)-frequency modulated (FM) signal contaminated by background noise, the instantaneous frequency (IF) retrieved via phase demodulation tends to fluctuate around its theoretical value. In this study, we first derive the influence of three key factors—carrier signal amplitude, amplitude modulation characteristics, and background noise variance—on the fluctuation (i.e., variance) of the estimated IF. Based on this theoretical insight, instantaneous angular speed (IAS) estimates derived from all vibration harmonics, together with their corresponding instantaneous IAS variance, can be estimated from the vibration signal. The optimal IAS estimate is then obtained by leveraging the maximum likelihood estimation (MLE) framework. Accordingly, this study proposes an enhanced IAS accuracy improvement (EIASAI) method for iterative refinement of IAS

estimation accuracy. The efficacy of the proposed method is evaluated and benchmarked against existing state-of-the-art methods using both numerical simulations and vibration signals collected from operational wind turbines.

**Keywords:** Instantaneous angular speed, Phase demodulation, Variable speed

## 1. Introduction

With the advancement of wind power technology, the demand for monitoring variable-speed equipment has been growing steadily. Owing to cost constraints, a large number of wind turbines are not equipped with speed reference sensors. Therefore, estimating IAS based on vibration signals themselves is highly essential[1].

Different types of tacholess IAS estimation methods can be categorized into spectrogram ridge extraction approaches[2] and phase-demodulation-based approaches[3]. Several strategies have been proposed to enhance the accuracy of the IAS estimated via spectrogram ridge extraction, such as adopting advanced time-frequency analysis methods[4,5], optimizing ridge extraction algorithms[6,7], and utilizing multiple harmonics for IAS estimation[8–12]. Compared with spectrogram ridge extraction approaches, phase demodulation-based methods are done by performing bandpass filtering on the vibration signal to extract a shaft-related mono-component AM-FM signal. On this basis, the IAS can be derived via the Hilbert transform[3,13] or the frequency-domain energy operator[14]. Consequently, phase demodulation-based methods exhibit a higher time resolution than their spectrogram ridge extraction counterparts. In addition, hybrid methods that integrate both principles have been proposed to further enhance the accuracy of IAS estimation[3,4].

The accuracy of the IAS estimated using a single harmonic can be compromised if the target harmonic is masked by noise over a local time period. To enhance the accuracy of IAS estimation via phase demodulation-based methods, Coats et al. [15] proposed a multi-stage speed estimation approach that iteratively selects higher-order harmonics for phase demodulation-based speed estimation. However, the criterion for selecting appropriate higher-order harmonics to improve IAS accuracy remains ambiguous and is highly dependent on empirical experience. Peng et al. [16] observed that impulsive noise is prone to occur during

the demodulation of planetary gearmesh (GM) harmonic for IAS estimation, regardless of the demodulation method employed. Further investigations revealed that such impulsive noise arises when the AM function approaches zero. To address this issue, the authors proposed a compensation strategy that replaces the noise-corrupted IAS estimates (at the time instances where impulsive noise occurs) with the IAS values estimated from uncorrupted high-order harmonics so that the IAS estimation accuracy can be improved. Furthermore, Peng et al. [17] investigated the effects of IAS estimation errors on order-tracked vibration signals, and proposed a set of evaluation indicators that enable the accuracy assessment of estimated IAS values without relying on a tachometer. Consequently, the accuracy of each IAS estimation result can be evaluated over short signal segments, which facilitates the improvement of overall IAS accuracy via the selection of the most reliable IAS values for individual segments. Subsequent studies[18] have demonstrated that the instantaneous error associated with the estimated IAS can be extracted from the order-tracked vibration signal, thereby enabling iterative calibration of the initial IAS estimate using the derived error. However, the selection of appropriate harmonics for IAS error estimation is dependent on expert experience, which restricts the practical implementation of this method in real-world applications. Peeters et al.[19] developed a multi-harmonic demodulation (MHD) method that incorporates multiple vibration components, and introduced the maximum likelihood estimation (MLE) framework into the method to assign optimal weights to the IAS estimates derived from different harmonics.

Aside from the end effect induced by the Hilbert transform, another critical observation is that the IF demodulated from a specific harmonic fluctuates consistently around its theoretical value when the target harmonic is corrupted by noise. However, the manner in which noise influences IF or IAS estimation has not been thoroughly discussed in existing studies. In this study, an analytical derivation is conducted to establish the relationship between IF fluctuation (i.e., variance) and three critical factors: noise variance, carrier signal amplitude, and the AM function. Based on these findings, we propose an Enhanced IAS accuracy improvement (EIASAI) method for iterative IAS refinement. This method is implemented through three key steps: first, introducing an optimal bandwidth selection strategy for IAS and IAS variance estimation; second, identifying the reliable regions of the estimated IAS and its corresponding variance; and finally, performing optimal IAS estimation and refinement. Compared with the

original IAS accuracy improvement (OIASAI) method [18], the primary advantage of the proposed EIASAI method lies in its ability to determine the point-wise reliability of each IAS estimate. Consequently, it eliminates the need for careful selection of appropriate harmonics and bandwidths during the IAS accuracy refinement process. The main contributions of this study are summarized as follows:

1. The relationship between the estimation variance of the IF/IAS and three key factors, namely background noise variance, carrier signal amplitude, and AM function, is theoretically derived.
2. Building upon these findings, an optimized bandwidth determination method for AM-FM harmonic extraction is proposed.
3. IAS from different harmonics can be integrated to enhance IAS estimation performance based on the estimated IAS variance.

The remainder of this paper is structured as follows. Section 2 elaborates on the mechanism by which background noise influences the IF/IAS estimated from AM-FM harmonics and validates this relationship. Section 3 discusses the overall strategy for refining IAS estimation based on the proposed method. Section 4 analyzes and compares the performance of the proposed method with that of existing methods, and finally, Section 5 presents the conclusions.

## 2. Influence of noise on phase demodulation of AM-FM harmonic

### 2.1 Signal model

A discrete AM-FM harmonic is defined as:

$$s(n) = C\big(1 + A(n)\big)\cos(\theta(n) + \phi_0) \tag{1}$$

where $C\big(1 + A(n)\big)$ denotes the discrete time-varying amplitude modulation ($C$ is a constant and $A(n) < 1$), $\theta(n)$ represents the instantaneous phase, and $\phi_0$ is the initial phase. The corresponding IF is calculated as:

$$\mathrm{IF}(n) = \frac{1}{2\pi} \cdot f_s\big(\theta(n) - \theta(n-1)\big) \tag{2}$$

with $f_s$ being the sampling frequency. The IF of $s(n)$ fluctuates within the interval $[f_1, f_2]$.

For real applications under variable-speed scenarios, vibration signals collected in practical scenarios typically consist of multiple AM-FM harmonics. Thus, bandpass filtering of the signal to extract mono AM-FM harmonic (within a specific frequency band) is always required before IF estimation by phase demodulation approach. For simplicity, the background noise is assumed to be additive white noise; after passing through an ideal bandpass filter (with passband $[f_3, f_4]$), the filtered noise is referred to as the band-limited white noise $w(n)$, which only retains frequency components within $[f_3, f_4]$. Statistically, $w[n] \sim \mathcal{N}(0, \sigma^2)$, where $\sigma^2$ is the noise variance. Therefore, the simulated signal corrupted by noise is then expressed as $x(n) = s(n) + w(n)$. Therefore, the analytic signal of $x(n)$ is constructed as:

$$\begin{aligned} \tilde{x}(n) &= \tilde{s}(n) + \tilde{w}(n) = \tilde{s}(n) + \Delta\tilde{s}(n) \\ &= C\big(1 + A(n)\big)e^{j(\theta(n)+\phi_0)} + w_{\mathrm{re}}(n) + jw_{\mathrm{im}}(n) \end{aligned} \tag{3}$$

where $w_{\mathrm{re}}(n)$ and $w_{\mathrm{im}}(n)$ are the real and imaginary parts of $\tilde{w}(n)$, respectively. Since $w[n]$ is band-limited white Gaussian noise, $w_{\mathrm{im}}(n)$ is also band-limited white Gaussian noise: $\mathcal{H}\{w[n]\} \sim \mathcal{N}(0, \sigma^2)$. In addition, since the Hilbert transform is a linear, orthogonal phase-shifting filter that preserves Gaussianity and independence for white noise, and thus $w[n]$ and $w_{\mathrm{im}}(n)$ are statistically independent.

**2.2 High local signal-to-noise (SNR) scenario**

When $C\big(1 + A(n)\big) \gg w(n)$ (i.e., the signal amplitude dominates the noise), the noisy analytic signal can be treated as a small perturbation $\Delta z$ added to the clean complex signal $z = |z|e^{j\phi}$. The phase change induced by $\Delta z$ is approximated via first-order Taylor expansion:

$$\arg(z + \Delta z) \approx \arg(z) + \frac{\partial \arg(z)}{\partial z}\Delta z + \frac{\partial \arg(z)}{\partial z^*}\Delta z^* \tag{4}$$

where $z^*$ denotes the complex conjugate of $z$. By computing the partial derivatives of $\arg(z)$ with respect to $z$ and $z^*$:

$$\frac{\partial \arg(z)}{\partial z} = \frac{-j}{2|z|^2}, \quad \frac{\partial \arg(z)}{\partial z^*} = \frac{j}{2|z|^2} \tag{5}$$

Substituting these derivatives into the Taylor expansion, the phase perturbation simplifies to:

$$\arg(z+\Delta z) \approx \arg(z) + \frac{\mathrm{Im}[z^* \cdot \Delta z]}{|z|^2} \tag{6}$$

Using Euler's formula, $\mathrm{Im}[z^* \cdot \Delta z]$ can be expressed as:

$$\mathrm{Im}[z^* \cdot \Delta z] = C\big(1+A(n)\big)[w_{\mathrm{im}}(n)\cos(\theta(n)+\phi_0) - w_{\mathrm{re}}(n)\sin(\theta(n)+\phi_0)] \tag{7}$$

Note that $|z|^2 = \big[C\big(1+A(n)\big)\big]^2$, the estimated phase $\hat{\phi}(n) = \arg(z+\Delta z)$ becomes:

$$\hat{\phi}(n) \approx \theta(n) + \phi_0 + \frac{w_{\mathrm{im}}(n)\cos(\theta(n)+\phi_0) - w_{\mathrm{re}}(n)\sin(\theta(n)+\phi_0)}{C\big(1+A(n)\big)} \tag{8}$$

The noise orthogonal component (the noise component orthogonal to the signal phase) is defined as:

$$w_{\perp}(n) = w_{\mathrm{im}}(n)\cos(\theta(n)+\phi_0) - w_{\mathrm{re}}(n)\sin(\theta(n)+\phi_0) \tag{9}$$

This simplifies the Eq.(8) to $\hat{\phi}(n) \approx \theta(n) + \phi_0 + \frac{w_{\perp}(n)}{C(1+A(n))}$.

The IF estimation is obtained by differentiating the estimated phase $\hat{f}(n) = \frac{f_s}{2\pi}\big[\hat{\phi}(n) - \hat{\phi}(n-1)\big]$. Comparing with the true IF $f(n) = \frac{f_s}{2\pi}[\theta(n) - \theta(n-1)]$, the frequency estimation deviation is derived as the difference between $\hat{f}(n)$ and $f(n)$.

$$\begin{aligned}
\Delta f(n) &= \frac{f_s}{2\pi}\big[\hat{\phi}(n) - \hat{\phi}(n-1)\big] - \frac{f_s}{2\pi}[\theta(n) - \theta(n-1)] \\
&= \frac{f_s}{2\pi}\left[\left(\theta(n) + \frac{w_{\perp}(n)}{\mathrm{C}\big(1+A(n)\big)}\right)\right. \\
&\quad \left. - \left(\theta(n-1) + \frac{w_{\perp}(n-1)}{\mathrm{C}\big(1+A(n-1)\big)}\right)\right] - \frac{f_s}{2\pi}[\theta(n) - \theta(n-1)] \\
&= \frac{f_s}{2\pi}\left[\frac{w_{\perp}(n)}{\mathrm{C}\big(1+A(n)\big)} - \frac{w_{\perp}(n-1)}{\mathrm{C}\big(1+A(n-1)\big)}\right]
\end{aligned} \tag{10}$$

In engineering applications, $A(n)$ is typically a slow-varying signal (i.e., $A(n) \approx A(n-1)$). This allows further simplification:

$$\Delta f(n) \approx \frac{f_s}{2\pi C\left(1+A(n)\right)}\left[w_\perp(n)-w_\perp(n-1)\right] = \frac{f_s}{2\pi C\left(1+A(n)\right)}\Delta w_\perp(n) \tag{11}$$

The orthogonal component of the band-limited white noise $w_\perp(n)$ remains a discrete band-limited signal. The variance of its first-order difference is (proof see Appendices A):

$$\mathrm{Var}[\Delta w_\perp(n)] = 2\mathrm{Var}[w_\perp(n)]\cdot\left[1-\rho_{w_\perp}(1)\right] \tag{12}$$

where $\rho_{w_\perp}(1) = \frac{\mathrm{Cov}[w_\perp(n),w_\perp(n-1)]}{\mathrm{Var}[w_\perp(n)]}$ denotes the first-order autocorrelation coefficient of $w_\perp(n)$.The autocorrelation function of $w_\perp(n)$ is:

$$R_{w_\perp}(k) = \mathrm{Cov}[w_\perp(n), w_\perp(n-k)] = \sigma^2\cdot\frac{\sin(\pi k f_c/f_s)}{\pi k f_c/f_s}\cdot\frac{\sin(\pi k(f_4-f_3)/f_s)}{\pi k(f_4-f_3)/f_s} \tag{13}$$

where $f_c = \frac{f_4+f_3}{2}$ is the center frequency of the bandpass filter. When the filter bandwidth $(f_4-f_3)$ is much smaller than $f_c$ (i.e., $f_4-f_3 \ll f_c$), the autocorrelation function approximates to $R_{w_\perp}(1) \approx \sigma^2\cdot\cos\left(2\pi\frac{f_c}{f_s}\right)$. Accordingly, the first-order autocorrelation coefficient simplifies to $\rho_{w_\perp}(1) \approx \cos\left(2\pi\frac{f_c}{f_s}\right)$. Therefore, Eq. (12) can be simplified as:

$$\begin{aligned}\mathrm{Var}[\Delta w_\perp(n)] &= 2\sigma^2\cdot\left[1-\cos\left(2\pi\frac{f_c}{f_s}\right)\right]\\ &= 2\sigma^2\cdot 2\sin^2\left(\pi\frac{f_c}{f_s}\right)\\ &= 4\sigma^2\sin^2\left(\pi\frac{f_c}{f_s}\right)\end{aligned} \tag{14}$$

Therefore, according to Eq. (11), the relationship between the variance of IF estimation, background noise, magnitude of the component and the amplitude modulation of the component can be expressed as:

$$\begin{aligned}\mathrm{Var}[\Delta f(n)] &= \left(\frac{f_s}{2\pi C\left(1+A(n)\right)}\right)^2 \cdot \mathrm{Var}[\Delta w_\perp(n)] \\ &= \frac{f_s^2}{4\pi^2 C^2\left(1+A(n)\right)^2} \cdot 4\sigma^2 \sin^2\left(\pi\frac{f_c}{f_s}\right) \\ &= \frac{f_s^2 \sigma^2 \sin^2\left(\pi\frac{f_c}{f_s}\right)}{\pi^2 C^2\left(1+A(n)\right)^2}\end{aligned} \tag{15}$$

**2.3 Low local SNR scenario**

When $A(n) \approx -1$ at specific time points, the noise term $w[n]$ dominates the signal component (i.e., $w[n] \gg C(1+A[n])$). In this case, Eq. (4) becomes invalid, and thus resulting the phase is dominated by noise:

$$\phi[n] = \arctan\left(\frac{C(1+A(n)\sin\left(\theta(n)+\phi_0\right)+w_{\mathrm{im}}(n)\}}{C(1+A(n)\cos(\theta(n)+\phi_0)\ \ +w_{\mathrm{re}}(n)}\right) \approx \arctan\left(\frac{w_{\mathrm{im}}(n)}{w_{\mathrm{re}}(n)}\right) \tag{16}$$

Let $X = w_{\mathrm{re}}(n)$ , $Y = w_{\mathrm{im}}(n)$, the joint probability density function (PDF) of $X$ and $Y$ (independent Gaussians) is:

$$f_{X,Y}(x,y) = \frac{1}{2\pi\sigma^2}\exp\left(-\frac{x^2+y^2}{2\sigma^2}\right), \quad (x,y) \in \mathbb{R}^2 \tag{17}$$

For the complex random variable $Z = X + jY$ (the analytic signal of the noise $\widehat{w}[n]$), we convert $(X,Y)$ to polar coordinates:

$$x = r\cos\phi, \quad y = r\sin\phi \tag{18}$$

where: $r[n] = \sqrt{X^2+Y^2}$ , $\phi[n] = \arctan\left(\frac{Y}{X}\right) = \arctan\left(\frac{w_{\mathrm{im}}(n)}{w_{\mathrm{re}}(n)}\right)$ . The Jacobian determinant of the transformation $(x,y) \to (r,\phi)$ is:

$$J = \begin{vmatrix}\frac{\partial x}{\partial r} & \frac{\partial x}{\partial \phi} \\ \frac{\partial y}{\partial r} & \frac{\partial y}{\partial \phi}\end{vmatrix} = \begin{vmatrix}\cos\phi & -r\sin\phi \\ \sin\phi & r\cos\phi\end{vmatrix} = r \tag{19}$$

Thus, $|J| = r$. Substitute the polar coordinates and Jacobian into the joint PDF:

$$f_{r,\theta}(r,\phi) = f_{X,Y}(r\cos\phi, r\sin\phi)\cdot|J| = \frac{r}{2\pi\sigma^2}\exp\left(-\frac{r^2}{2\sigma^2}\right) \tag{20}$$

By integrating the joint PDF over $r$ (the magnitude, $r \geq 0$), we proceed to derive the probability distribution of instantaneous phase $\phi[n]$:

$$f_{\phi}(\phi) = \int_0^{\infty} f_{r,\phi}\,(r,\phi)dr = \int_0^{\infty} \frac{r}{2\pi\sigma^2} exp\left(-\frac{r^2}{2\sigma^2}\right) dr \tag{21}$$

Let $u = \frac{r^2}{2\sigma^2}$, so $du = \frac{r}{\sigma^2}dr$. The integral simplifies to:

$$f_{\phi}(\phi) = \frac{1}{2\pi}\int_0^{\infty} \exp\,(-u)du = \frac{1}{2\pi} \tag{22}$$

Therefore, the probability density function of the instantaneous phase $f_{\phi}(\phi) = \frac{1}{2\pi}$ holds for $\phi \in [0,2\pi)$, so that $\phi[n]$ follows a uniform distribution over the interval $[0,2\pi)$, leading to its derivative $\hat{f}(n) = \frac{f_s}{2\pi}\left[\hat{\phi}(n) - \hat{\phi}(n-1)\right]$ being completely random.

**2.4 Explanation validation**

To validate the aforementioned theoretical analysis, a gear vibration simulation is performed. Specifically, the IAS of the shaft under study is first simulated, and the IAS is integrated to obtain the rotational angle $\theta(n)$ (in radians) of the shaft. The GM vibration is defined as:

$$s(n) = \sum_{k=1}^{K} C_k\,[1 + A_k(n)]\cos(kZ\theta(n) + \phi_k) \tag{23}$$

where $k$ denotes the harmonics of the GM component, $Z$ is the number of teeth of the gear; $C_k$ is the amplitude of the $k^{\text{th}}$ vibration harmonic, and $\phi_k$ is the initial phase of the harmonic.

The term $A_k(n)$ serves as the AM function for the GM force and is expressed as:

$$A_k(n) = \sum_{m}^{M}\left[a_{k,m}\cos\left(m\theta(n) + \gamma_{k,m}\right)\right] \tag{24}$$

where $a_{k,m}$ and $\gamma_{i,m}$ are amplitude coefficient and initial phase for $m^{\text{th}}$-order harmonic, respectively. Therefore, the final simulated signal can be expressed as the sum of $x(n)$ and additive white noise $w(n)$.

The first six GM harmonics are simulated with distinct amplitude modulation functions, and

**错误!未找到引用源。** provides the key parameters. In addition, sampling frequency $f_s = 1000$ Hz, signal duration $T = 5$ s and IAS increases linearly from 2 Hz to 2.04 Hz, i.e., the IF of first GM component varies from 50 Hz to 51 Hz.

Table 1: Parameters used for the simulation

| Parameter | Value(s) | Parameter | Value(s) |
|---|---|---|---|
| $a_{1,1}$-$a_{6,1}$ | 0.5,0.3,0.4,0.3,0.6,0.2 | $m$ | 2,4 |
| $a_{1,2}$-$a_{6,2}$ | 0.3,0.2,0.5,0.3,0.2,0.4 | $\gamma, \phi$ | $\mathcal{U}(-\pi, \pi)$ |
| $C_1 - C_6$ | 5,2,4,1,3,2 | $Z$ | 25 |

The IF, time domain waveform, the term $\frac{1}{C_1^2(1+A_1(n))^2}$ and spectrum of this signal are presented in Figure 1.

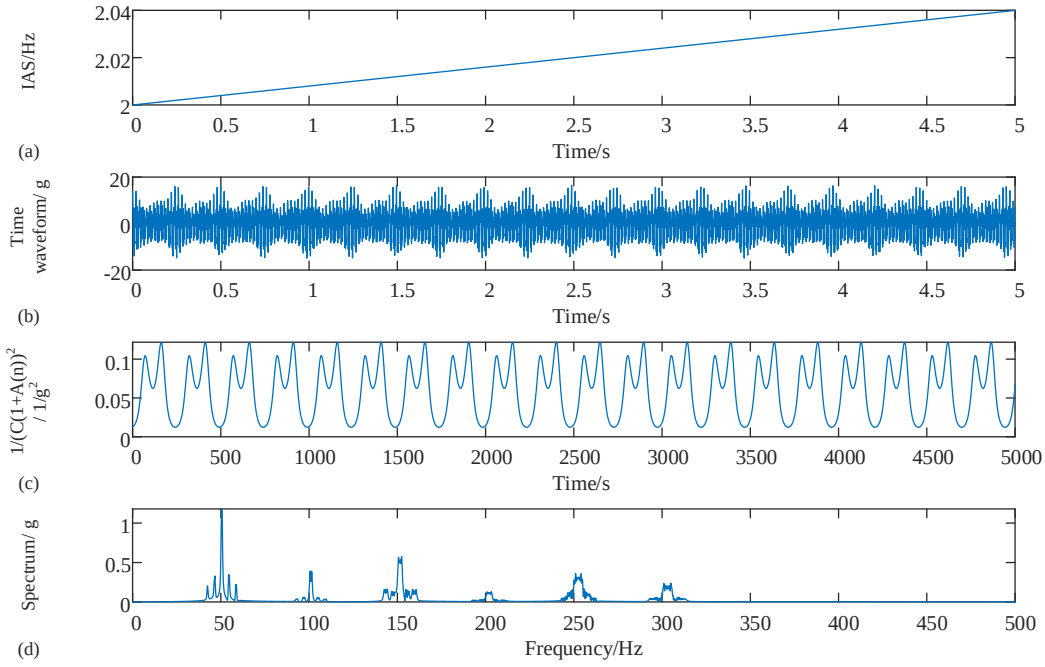


Figure 1 (a) IAS, (b) time waveform, (c) $\frac{1}{C_1^2(1+A_1(n))^2}$ and (d) spectrum of the simulated signal.

### 2.4.1 Influence of noise variance on IF estimation

To investigate the impact of noise variance on IF estimation, white noise $w(n)$ with different variance values (1, 9, 25,48,81) are used. $x(n)$ is filtered using a bandpass filter with

passband [40, 60] Hz) first so that the first GM component is extracted. The IF is then estimated by phase demodulating the bandpass filtered signal. In addition, the noise orthogonal component $w_{\perp}(n)$ (Eq. (4)) is computed concurrently. To quantify the point-wise actual IF variance and point-wise noise variance $\mathrm{Var}[\Delta w_{\perp}(n)]$ for theoretical IF variance calculation, $s(n)$ is held constant throughout the experiment while a total of 100 independent realizations of white Gaussian noise for each noise variance level are made.

Figure 2 presents the comparison between the theoretical IF and IF estimates under different white noise variance levels and the comparison between the actual IF estimation versus its theoretical counterpart. When SNR is high enough (e.g., noise variance <25 in this case), the actual variance of IF closely matches its theoretical variance. Additionally, both of them show a linear relationship with $\frac{1}{C_1^2(1+A_1(n))^2}$ shown in Figure 1 (c), which aligns with the theoretical derivation in Section 2.2.

As the noise variance increases, the IF estimates exhibit increasingly severe fluctuations. This observation is consistent with the expectation that stronger noise introduces greater perturbations to the phase demodulation process. When the noise variance reaches a certain level (e.g., noise variance = 49) for this case, the instantaneous phase (in partial time regions) becomes noise-dominated in partial time regions. As discussed in Section 2.3, such noise dominance leads to completely random IF estimates in these regions. Furthermore, the occurrence frequency of these random regions increases with the noise variance. Consequently, the actual IF variance deviates significantly from the theoretical variance under high-noise conditions.

**2.4.2 Influence of carrier signal amplitude on IF estimation**

To investigate the influence of the carrier signal amplitude (regulated by the constant amplitude coefficient $C$) on IF estimation, the constant amplitude coefficient $C_1$ has been adjusted from its initial value of 5 (as listed in Table 1) to different levels (1, 3, 5, 7, 9). The white noise $w(n)$ with a variance of 25 is employed for the completed signal simulation. $x(n)$ is filtered using a bandpass filter with a passband of [40, 60] Hz, followed by IF estimation via phase demodulation. For each value of constant amplitude coefficient, 100 independent

simulations of the noisy signal are conducted to calculate both the actual and theoretical IF estimation variance.

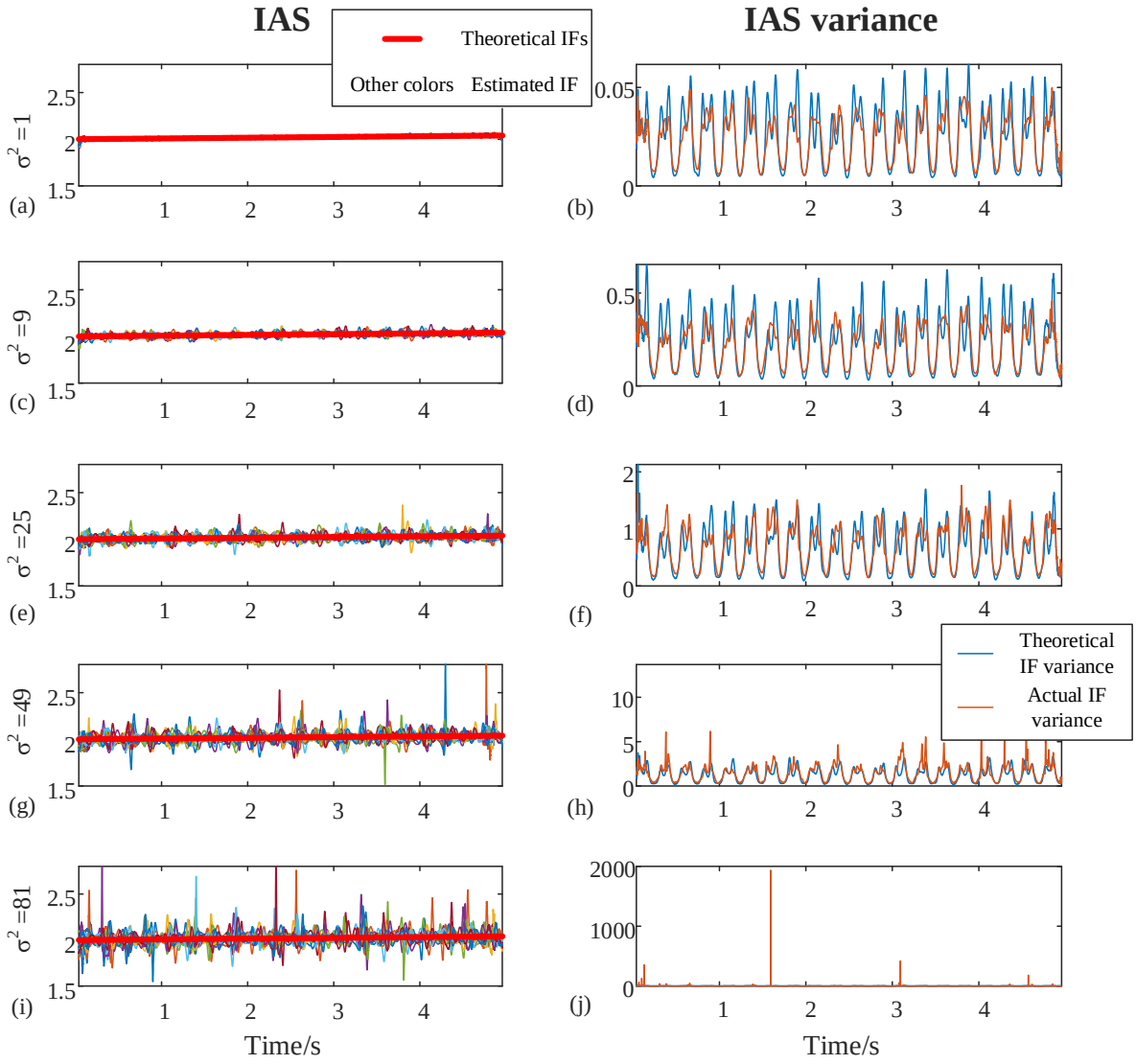


Figure 2 Comparisons of theoretical and actual IF (left panel) and IF variance (right panel) for Gaussian white noise variances of (a, b) 1, (c, d) 9, (e, f) 25, (g, h) 49, and (i, j) 81.

The IF estimates and their variances (both theoretical and actual values) are presented in Figure 3. It can be observed that as the amplitude of the carrier signal increases, the IF estimates become increasingly accurate, and the variance of the IF estimates decreases accordingly. For low carrier signal amplitudes (corresponding to low SNR), low local SNR regions emerge more frequently; this leads to a deviation between the actual IF variance and the theoretical prediction.

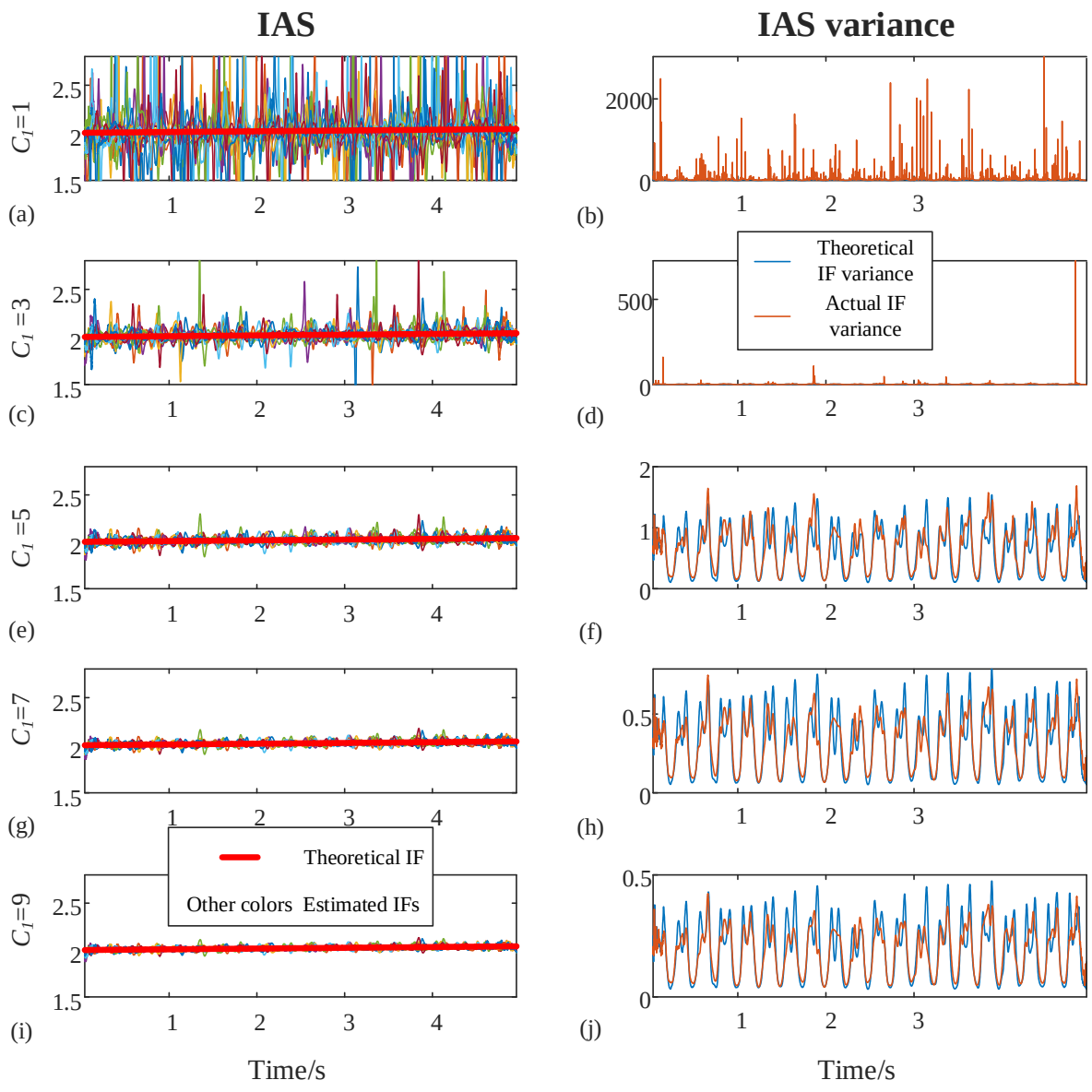


Figure 3 Comparisons of theoretical and actual IF (left panel) and IF variance (right panel) for the amplitude of the first GM component of (a, b) 1, (c, d) 3, (e, f) 5, (g, h) 7, and (i, j) 9.

### 2.4.3 Influence of amplitude modulation (bandwidth) on IF estimation

To investigate the effect of AM function $A(n)$ on IF estimation, different passbands ($[48,53]$ Hz, $[43,58]$ Hz, and $[45,60]$ Hz) are applied to the simulated signal generated according to Table 1 with white noise (variance=25). These filters selectively retain distinct signal components, as specified below:

$[48,53]$ Hz: Retains only the carrier component (no amplitude modulation).

[43,58] Hz: Retains the first sub-component $A_1(n) = a_{1,2}\cos\left(2\theta(n) + \gamma_{1,2}\right)$;

[45,60] Hz and [45,60] Hz : Retains both sub-components of $A_1(n) = \sum_m^M\left[a_{1,m}\cos\left(m\theta(n) + \gamma_{1,m}\right)\right]$.

Correspondingly, the AM term involved in the theoretical IF variance calculation—i.e., $A(n)$ in Eq. (15)—has been adjusted. For each filter configuration, 100 independent simulations were performed to compute both the theoretical and actual IF variances.

Figure 4 presents the IF estimates along with their theoretical and actual variances. As the filter passband narrows (i.e., more components of $A(n)$ are filtered out), the impact of amplitude modulation on IF estimation gradually diminishes. Consequently, the accuracy of IF estimation improves incrementally, while the IF variance decreases. Compared with the latter two passbands (both of which include all AM components), a wider passband admits more noise, thereby increasing the uncertainty of IF estimation. Despite this, the actual IF variance is consistent with the theoretical IF variance in most cases.

These results validate the theoretical derivation of IF fluctuations (Eq. (15)) under different carrier signal amplitudes, amplitude modulations, and noise interferences. It can thus be concluded that the amplitude of the AM-FM component ($C$) is positively correlated with the accuracy of IF estimation and negatively correlated with the IF variance. In contrast, the noise variance ($\sigma^2$) and the strength of the amplitude modulation term $A(n)$ exhibit the opposite trends.

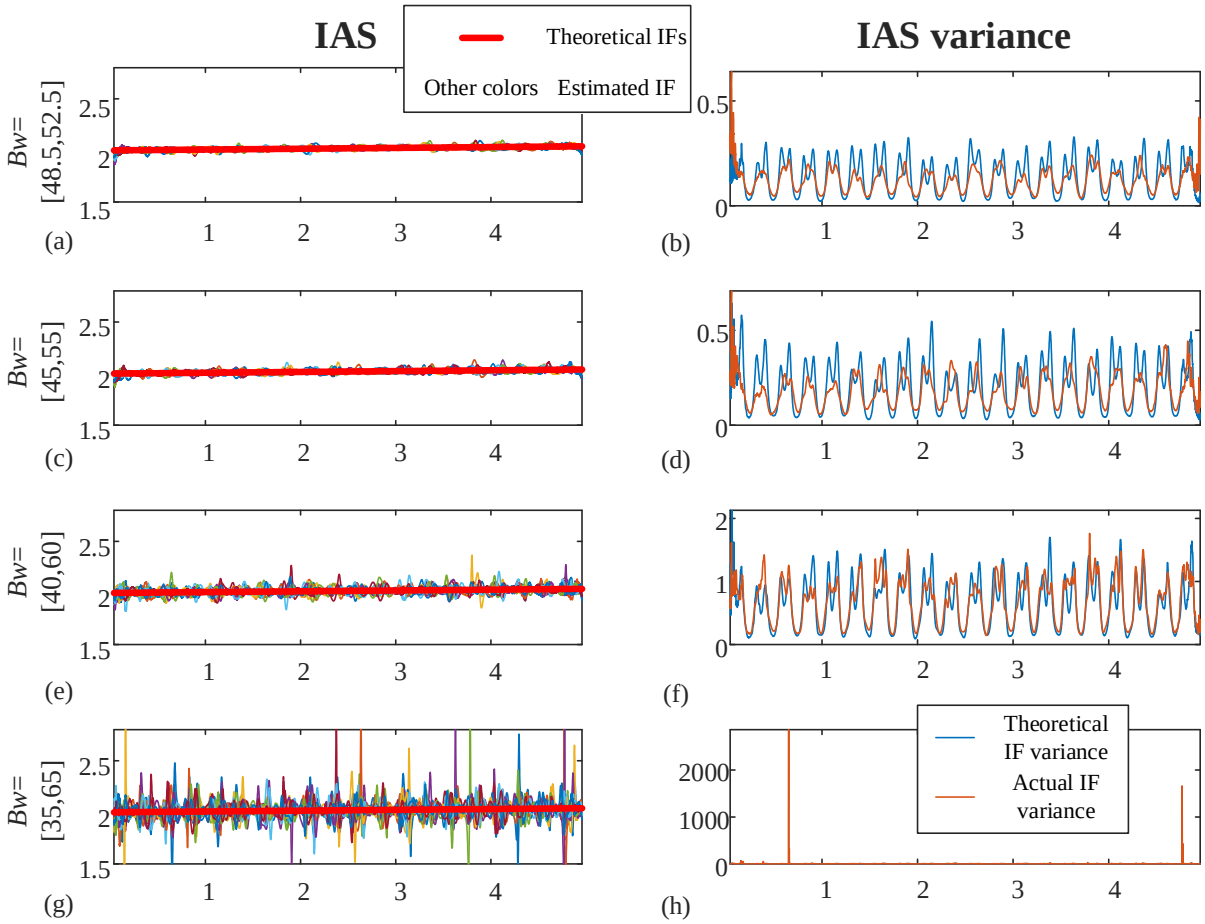


Figure 4 (left) Comparison between theoretical and actual IF and (right) Comparison between theoretical and actual IF variance when passband of the filter is (a) and (b) [48.5,52.5]; (c) and (d) [45,55]; (e) and (f) [40,60]; (g) and (h) 7; (i) and (j) [35,65].

## 3. Proposed method

For vibration signals collected from real variable speed applications, they typically consist of multiple AM-FM components. Thus, several IAS estimations with different accuracy can be calculated by phase demodulating different mono AM-FM components. Supporting $o$ to be the harmonic number and $K$ be the the total number of harmonics, IAS estimations $\widehat{IAS}_1, \ldots \widehat{IAS}_k, \ldots, \widehat{IAS}_K$ follow Gaussian distributions $\widehat{IAS}_k \sim N(IAS_{\text{true}}, \sigma_k^2)$. Therefore, the optimal $\widehat{IAS}_{opt}$ can be obtained by using maximum likelihood estimation (MLE) if all of the $\widehat{IAS}_k$ and $\sigma_k^2$ can been calculated.

For vibration signals collected from real variable-speed applications, multiple AM-FM harmonics are typically involved. Consequently, several IAS estimates with varying accuracy can be obtained by phase-demodulating different single AM-FM components. Let $k$ denote the harmonic number and $K$ represent the total number of harmonics; the IAS estimates $\widehat{IAS}_1, \ldots \widehat{IAS}_k, \ldots, \widehat{IAS}_K$ follow Gaussian distributions, i.e., $\widehat{IAS}_k \sim N(IAS_{\text{true}}, \sigma_k^2)$. Therefore, the optimal estimate $\widehat{IAS}_{opt}$ can be derived via maximum likelihood estimation (MLE) if all $\widehat{IAS}_k$ and $\sigma_k^2$ are available.

Based on Eq. (15) and Section 2.3, the following factors should be considered to improve the estimation accuracy of each $\widehat{IAS}_k$ and its variance $\sigma_k^2$:

**1. Optimization of filter bandwidth**: This aims to minimize the adverse effects of noise and amplitude modulation on IF estimation. Ideally, the optimal passband should only cover the frequency range corresponding to frequency modulation, while excluding amplitude modulation components—provided that these two types of components can be separated in the frequency/order domain. For vibration signals, the IF of AM sidebands and the IF of the carrier signal are generally correlated with the rotational speed (e.g., gear meshing components and their sidebands). Thus, if an IAS estimate (denoted as $\text{IAS}_o(t)$) is sufficiently accurate ($\text{IAS}_o(t) \approx \text{IAS}_{\text{True}}(t)$), the carrier signal can be distinguished from its AM sidebands after order tracking of the signal [18].

**2. Elimination of the impact of low local SNR regions in each AM-FM harmonic**: IAS estimates and their variances are completely random in such regions, which will reduce the accuracy of $\widehat{IAS}_{opt}$ in the subsequent process. Therefore, regions where the AM-FM harmonic experiences low local SNR must be identified and excluded from further analysis.

In addition, as a supplementary scheme for further improving IAS estimation accuracy, the proposed method requires a rough IAS estimation in advance. The signal must undergo order tracking to enable the distinction of all harmonics; subsequent data processing is therefore primarily conducted in the angle domain. It should be noted that $IF(n)$ and $IAS(n)$ referenced in the following steps do not represent the IF or IAS. Instead, they correspond to the estimation errors in the angle domain [18].

The overall strategy for enhancing IAS estimation consists of four main steps: (1) Optimal

bandwidth determination and harmonic selection; (2) Low local SNR region identification and IAS variance estimation; and (3) Optimal IAS estimation and refinement.

### 3.1 Optimal bandwidth determination and harmonics selection

Since different harmonics exhibit distinct AM characteristics, the passbands used for individual harmonics need to be adaptively determined. Inspired by Ref. [20], which recursively employs a power spectral density (PSD) estimator for telescoping spectral estimation, this study proposes a recursive optimal bandwidth determination method. The core objective of this method is to maximally exclude AM sidebands for each individual harmonic.

The adaptive bandwidth determination method for a single harmonic $k$ is detailed as follows:

1. Obtain the data sample $x(n)$ for $n = 0, \ldots, N-1$.

2. Set the iteration index $m = 0$. Initialize the Band of Interest (BOI) as $Bw(m) = [k - c_1 k, k + c_1 k]$, where $c_1$ is a constant ($c_1 = 0.05$ in this study to ensure a sufficiently wide initial passband). Define the PSD length as $N_w = c_2 k$, where $c_2$ is a constant (determined by the harmonic $k$, a minimum value of $\min(N_w) \geq 100$ is recommended). $c_3 = 70$ (PSD noise threshold parameter, used in Step 5) and $c_4 = 0.01$ (termination condition constant, used in Step 11).

3. Apply bandpass filtering, down-conversion, and decimation to $x(n)$ using $Bw(m)$, yielding the zero-centered, bandwidth-optimized signal $y(i)$.

4. Estimate the PSD of $y(i)$, denoted as $\mathcal{P} = \{p_1, p_2, \ldots, p_{N_w}\}$.

5. Set the PSD noise threshold as the value corresponding to the $c_3\%$ largest element in $\mathcal{P}$. To avoid boundary misjudgment, the threshold is adjusted as: $\text{thre}_{psd} = \left(\text{sort}_{\uparrow}(\mathcal{P})\right)_{\lfloor c_3 \cdot N_w + 0.5 \rfloor} - 10^{-9}$, where $\text{sort}_{\uparrow}(\mathcal{P})$ denotes the ascending sorted sequence of $\mathcal{P}$.

6. Set $e = 1$. For each $j \in [1, N_w]$:

   If $p(j) < \text{thre}_{psd}$ and $p(j-1) \geq \text{thre}_{psd}$, record the left BOI boundary $B_{m,l}(e) = j$. If $p(1) < \text{thre}_{psd}$, set $B_{m,l}(1) = 1$.

If $p(j) \geq 0$ and $p(j-1) < 0$, record the right BOI boundary $B_{m,r}(e) = j$. If $p(N_w) < \text{thre}_{psd}$, set $B_{m,r}(e) = N_w$.

Increment $e$ by 1 ($e \leftarrow e + 1$).

7. Retain the BOI $[B_{1,l}, B_{1,r}]$ from the first iteration ($m = 1$) for subsequent SNR calculation and IAS error variance estimation (Section 3.2).
8. To mitigate the over-determination caused by a high $\text{thre}_{psd}$, update the adjacent BOI boundaries to their midpoint:

$$B_{m,r}(e-1), B_{m,l}(e) = \frac{B_{m,r}(e-1) + B_{m,l}(e)}{2} \tag{24}$$

9. Remove weak BOIs. For each BOI, compute its peak PSD value: $\text{Peak}(e) = \max_{j=B_{m,l}(e)}^{B_{m,r}(e)} p_j$. Set the peak threshold $\text{thre}_{peak} = e^{\text{quantile}(\ln(\text{max\_Peak}),\, 0.5)}$ and retain only valid BOIs that satisfy $\text{Peak}(e) > \text{thre}_{\text{peak}}$}.
10. Update the bandwidth $Bw(m) = [B_{m,l}, B_{m,r}]$ if $B_{m,l} < o < B_{m,r}$; otherwise, terminate the algorithm.
11. If $B_{m,r} - B_{m,l} > c_4 k$, set $m \leftarrow m + 1$ are return to Step 3; otherwise, stop the iteration.

After determining the adaptive bandwidth for all harmonics, a subset of high-SNR harmonics is selected for subsequent processing. This step improves computational efficiency and avoids the negative adverse effects of low-SNR harmonics on the accuracy of IAS estimation. The SNR of harmonic $k$ is computed as:

$$\text{SNR}_k = \frac{\sum_{e=1}^{E} \sum_{f=B_{1,l}(e)}^{B_{1,r}(e)} |X(f)|^2}{\sum_{f=Bw(0)} |X(f)|^2 - \sum_{e=1}^{E} \sum_{f=B_{1,l}(e)}^{B_{1,r}(e)} |X(f)|^2} \tag{25}$$

Once the SNR of each harmonic is obtained, the harmonic selection criteria are defined as follows: set the SNR threshold as $\text{thre}_{\text{SNR}} = e^{\text{quantile}(\ln(\text{SNR}),\, 0.5)}$, and initially retain all harmonics that satisfy $\text{SNR}_k > \text{thre}_{\text{SNR}}$. To further reduce the computational burden, if the number of initially selected harmonics $K$ exceeds 5, only the top 5 harmonics with the highest $\text{SNR}_k$ values are retained for subsequent analysis.

**3.2 Low Local SNR Regions identification and IAS variance estimation**

In general, the derivative of the IF, i.e., the instantaneous acceleration is a slowly varying function ($\dot{IF} \approx 0$), especially when the signal is order-tracked (where frequency modulation induced by speed fluctuations has been eliminated). However, when the AM term $1 + A_k(n)$ of harmonic $k$ approaches 0, the IF will exhibit abrupt variations, as elaborated in Section 2.2, resulting in its derivative deviating significantly from 0 ($\left|\dot{IF}\right| \gg 0$).

Owing to discrepancies in carrier signal intensity, amplitude modulation, and noise intensity across different harmonics, those harmonics subjected to stronger noise or satisfying $|A_k(n)| \to 1$ will undergo more frequent distortions in their instantaneous phase, frequency, and acceleration. Therefore, IF candidates must be considered collectively to identify regions with low local SNR. First, the instantaneous acceleration magnitude of harmonic $k$ is calculated and normalized by the corresponding harmonic order, yielding $|IA(k,n)| = \frac{|\dot{IF}(k,n)|}{k}$. All spatiotemporal regions $(k,n)$ across harmonics that satisfy $|IA(k,n)| > e^{\text{quantile}(\ln(|IA(k,n)|),\,0.9)}$ are designated as low local SNR regions.

Once these low local SNR regions are detected and excluded, the variance of the IF estimated from harmonic $k$ within high local SNR regions can be computed. The exact calculation of $\text{Var}[\Delta w_\perp(n)]$ (Eq. (14)) requires the noise variance for each time interval $n$, which is impractical for real-world applications. Thus, an approximate estimation of $\text{Var}[\Delta w_\perp(n)]$ must be derived directly from $w(n)$ itself (see Appendix B). For simplicity, the noise $w(n)$ surrounding harmonic $k$ is defined as the bandpass-filtered signal with the passband (Section 3.1, Step 7). The orthogonal noise component $w_\perp(n)$ can then be obtained via Eq. (9), where $\theta(n) = 2\pi T_s \int_0^N IF(n)dn$. $\text{Var}[\Delta w_\perp]$ is subsequently derived by differentiating $w_\perp(n)$ and calculating the variance of the resulting derivative.

The amplitude modulation of harmonic $k$ ($AM_k(n)$) can be acquired by amplitude demodulation of the signal filtered with the passband $Bw(m)$. Therefore, the variance of the IAS estimated from harmonic $k$ can be calculated as:

$$\sigma_k^2 = Var[\Delta IAS_k] = \text{Var}\left[\frac{\Delta IF_k}{k}\right] = \left(\frac{f_s}{2\pi k AM_k(n)}\right)^2 \cdot \text{Var}[\Delta w_{\perp \text{k}}] \tag{26}$$

**3.3 Optimal IAS estimation and refinement**

Given $K$ harmonic IAS estimates derived from individual harmonics, denoted as $\widehat{IAS}_1, \widehat{IAS}_2, \ldots, \widehat{IAS}_K$, each estimate follows a normal distribution $\widehat{IAS}_k \sim \mathcal{N}(IAS_{\text{true}}, \sigma_k^2)$. Since these estimates are mutually independent, the joint likelihood function is constructed as:

$$L(IAS) = \prod_k^K f\left(\widehat{IAS}_k \mid IAS\right) = \prod_k^K \frac{1}{\sqrt{2\pi}\sigma_k} \exp\left(-\frac{\left(\widehat{IAS}_k - IAS\right)^2}{2\sigma_k^2}\right) \tag{27}$$

and the log likelihood yields:

$$\ln L(IAS) = -\frac{K}{2}\ln(2\pi) - \sum_k^K \ln \sigma_i - \frac{1}{2}\sum_k^K \frac{\left(\widehat{IAS}_i - IAS\right)^2}{\sigma_k^2} \tag{28}$$

To find the optimal estimate, we take the derivative of $\ln L(IAS)$ with respect to $IAS$ and set it to zero:

$$\frac{d}{dIAS}\left(-\frac{1}{2}\sum_k^K \frac{\left(\widehat{IAS}_i - IAS\right)^2}{\sigma_k^2}\right) = \sum_k^K \frac{\widehat{IAS}_k - IAS}{\sigma_k^2} = 0 \tag{29}$$

Rearranging the above equation, the optimal estimate is derived as:

$$IAS_{\text{opt}}(n) = \frac{\sum_k^K \frac{\widehat{IAS}_k}{\sigma_k^2}}{\sum_k^K \frac{1}{\sigma_k^2}} \tag{30}$$

Since the vibration signal is first order tracked using the rough IAS estimate $IAS_o(t)$, all the aforementioned operations are implemented on the angle-domain vibration signal. The obtained optimal $IAS_{\text{opt}}(n)$ actually represents the fluctuation estimate of the IAS in the angle-domain. Accordingly, it is necessary to convert the result back to the time domain via reverse order tracking, and then multiply it by $IAS_o(t)$ to yield the time-domain IAS fluctuation $IAS_{\text{opt}}(t)$. The IAS can thus be updated to enhance its estimation accuracy [18]:

$$IAS_u(t) = IAS_o(t)\left[1 + \text{Re\_Order\_track}\left(IAS_{\text{opt}}(\text{n})\right)\right] \tag{31}$$

## 4. Validation

Three different scenarios, including simulation and two wind turbine dataset, are employed to evaluate and compare the performance of the proposed method against existing state-of-the-art methods..

### 4.1 Simulation

The variable-speed vibration signal is generated using the simulation framework elaborated in Section 2.4. Key parameters were configured as follows: sampling frequency $f_s = 5000$ Hz, signal duration $T = 120$ s, and IAS varying from 2 Hz to 5 Hz. The 3rd harmonic is intentionally designed to be asynchronous with the IAS. Additive white Gaussian noise is superimposed to achieve an SNR of -5 dB, thereby mimicking low-SNR conditions encountered in real-world applications. The time domain waveform, frequency spectrum, and spectrogram of the simulated signal are presented in Figure 5.

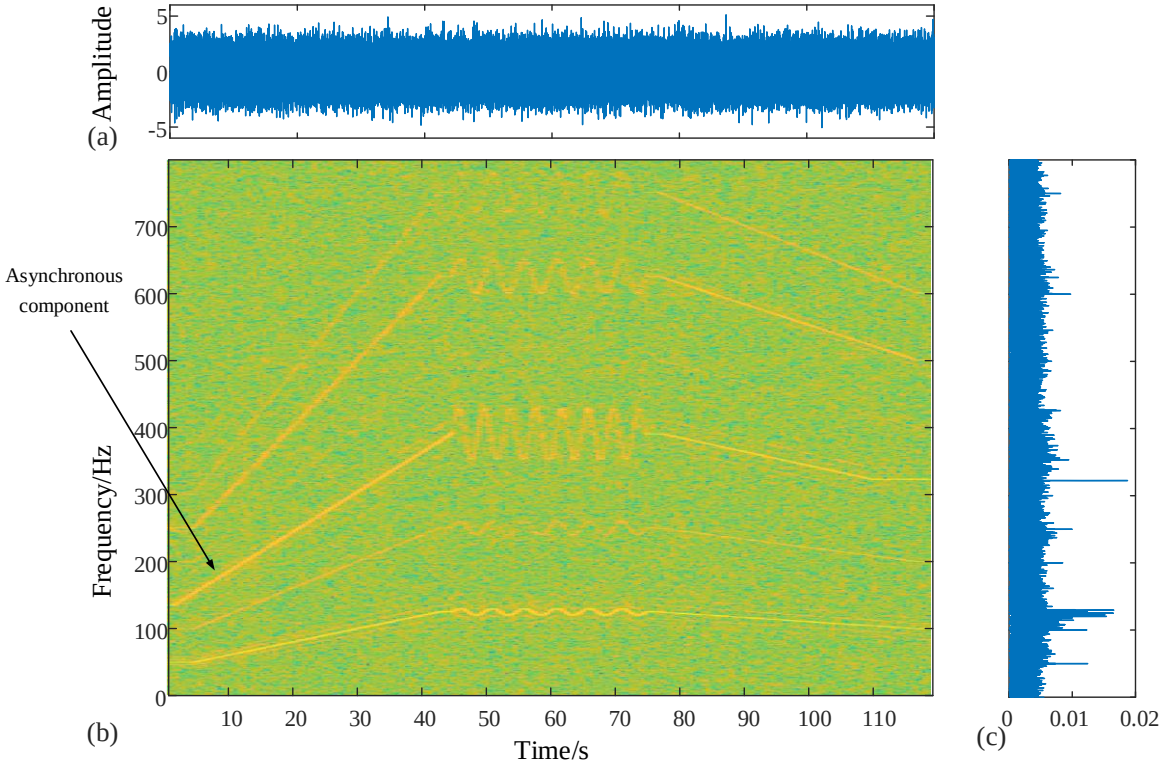


Figure 5 (a) Time waveform, (b) spectrogram and (c) spectrum of the simulated signal.

The ridge of the first GM harmonic is extracted from the spectrogram to obtain an initial rough estimate of the IAS. Both the EIASAI method and original IAS accuracy improvement method (OIASAI), along with the MHD, are applied to the simulated signal for comparative analysis. A summary of the input parameters employed is presented in Table 2. The OIASAI method is tested under two distinct harmonic candidate schemes: the first scheme selects the three shaft-synchronous harmonics with the largest amplitudes for IAS estimation enhancement, while the second scheme utilizes all available harmonics for the same purpose.

Table 2: Parameters used for IAS estimation of the simulated signal

| Parameter | EIASAI | OIASAI -1 | OIASAI -2 | MHD |
|---|---|---|---|---|
| Fundamental harmonic/$h$ | 25 | 25 | 25 | 25 |
| Sampling order/ $Os$ | 400 | 400 | 400 | |
| Used harmonics /$k$ | $h*\left\lfloor 1{:}\frac{Os}{2h}\right\rfloor$ | $h*[1,2,4]$ | $h*\left\lfloor 1{:}\frac{Os}{2h}\right\rfloor$ | $h*\left\lfloor 1{:}\frac{Os}{2h}\right\rfloor$ |
| Initial passband | $0.9k, 1.1k$ | $k-0.15\sqrt{k}, k+0.15\sqrt{k}$ | $k-0.15\sqrt{k}, k+0.15\sqrt{k}$ | 3 |

The IAS estimates derived from different methods, along with their corresponding IAS estimation errors, are presented in Figure 6. It can be observed that the EIASAI method yields the most accurate IAS estimates, as its time-varying error is the smallest. In contrast, the OIASAI method treats IAS deviations across all employed components uniformly; consequently, OIASAI-2— which incorporates asynchronous components—suffers from degraded IAS estimation accuracy, resulting in the poorest performance among all the compared methods.

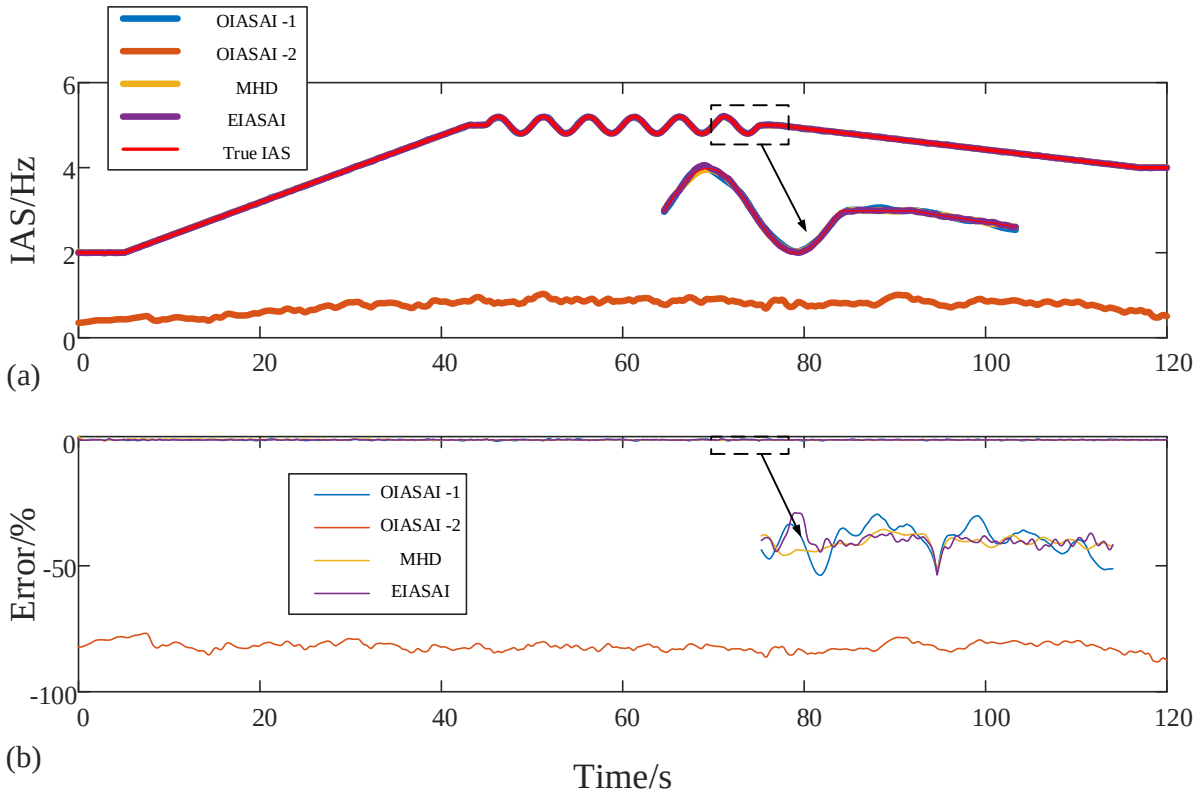


Figure 6 (a) Actual IAS and IAS estimated by different methods and (b) their corresponding error.

To further evaluate the performance of different methods in improving IAS estimation accuracy, the mean absolute error (MAE) and L1L2 norms across all iterations for each method are presented in Figure 7. Among the evaluated approaches, OIASAI-2 is the only one that fails to outperform the initial rough IAS estimate—a shortcoming attributable to its suboptimal harmonic selection and IAS refinement strategy. In contrast, while OIASAI-1 (MAE: 0.11%) relies on shaft-synchronous harmonics for IAS estimation, both the EIASAI method (MAE: 0.04%) and the MHD method (MAE: 0.08%) assign weights to individual IAS estimates $\widehat{IAS}_k$ via distinct strategies, thereby yielding more accurate results. The superior accuracy of EIASAI originates from its focus on harmonics with the highest SNR for optimal IAS estimation and refinement, which effectively avoids interference from low-SNR harmonics. Additionally, the adoption of an adaptive optimal bandwidth for the EIASAI method further contributes to its superior performance over alternative approaches. Notably, equivalent performance evaluation results can be obtained without relying on a tachometer, as the variation trends of the L1L2 norms are analogous to those of the MAE.

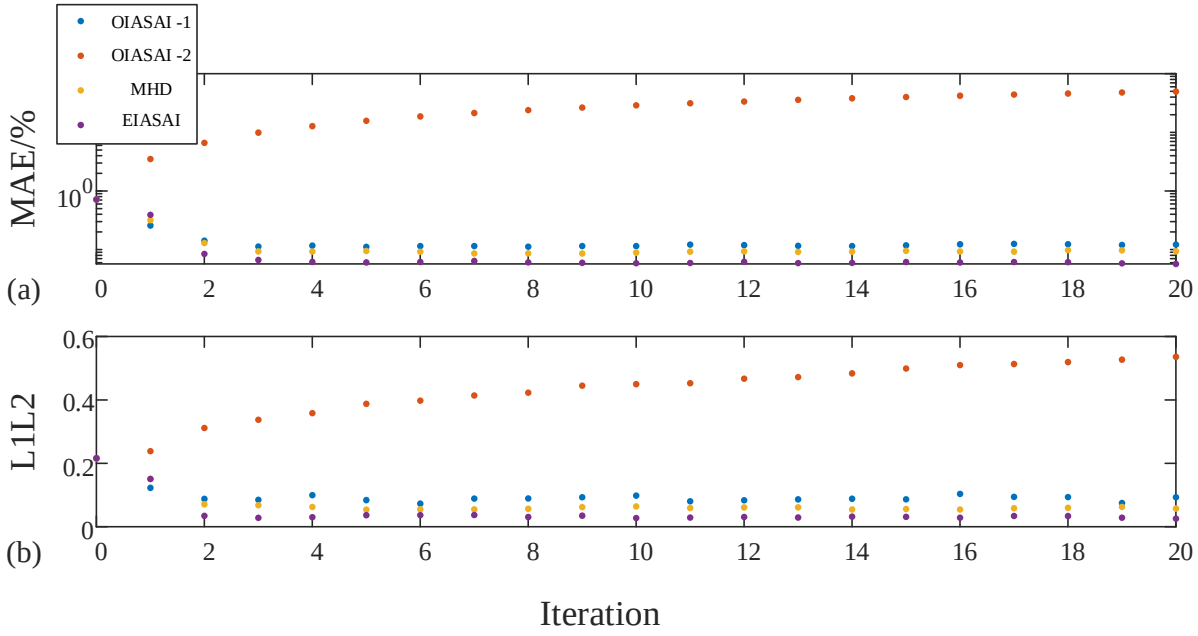


Figure 7 (a) MAE and (b) L1L2 of the estimated IAS in each iteration.

### 4.2 Wind turbine gearbox dataset 1

Wind Turbine Dataset 1, first released in conjunction with the 2014 International Conference on Condition Monitoring of Machinery in Non-Stationary Operations [21],

comprises vibration signals acquired from the gearbox housing of a 2 MW wind turbine (designated as WT1). The measurement points are positioned in the vicinity of the planetary gear stage of the gearbox. The kinematic configuration of the gearbox is shown in Figure 8. This dataset encompasses a 550-second vibration signal segment, acquired at a sampling frequency of 5000 Hz. A reference rotational speed signal, acquired via an angle encoder, is additionally provided for subsequent validation. The instantaneous angular speed (IAS) of the planet carrier, time-domain waveform, frequency spectrum, and spectrogram of this signal are presented in Figure 9.

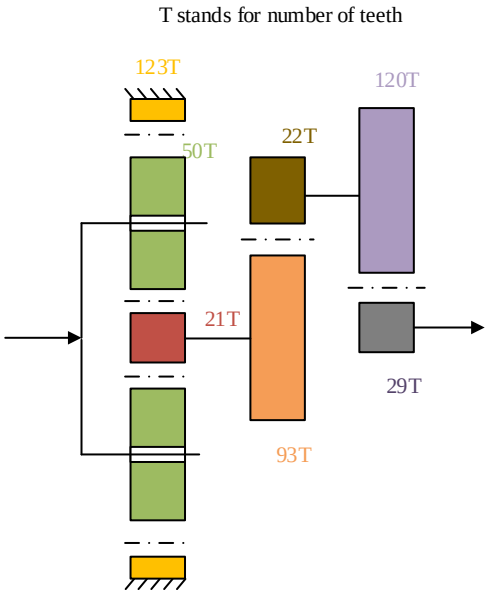


Figure 8: Kinematic configuration of the wind turbine dataset 1.

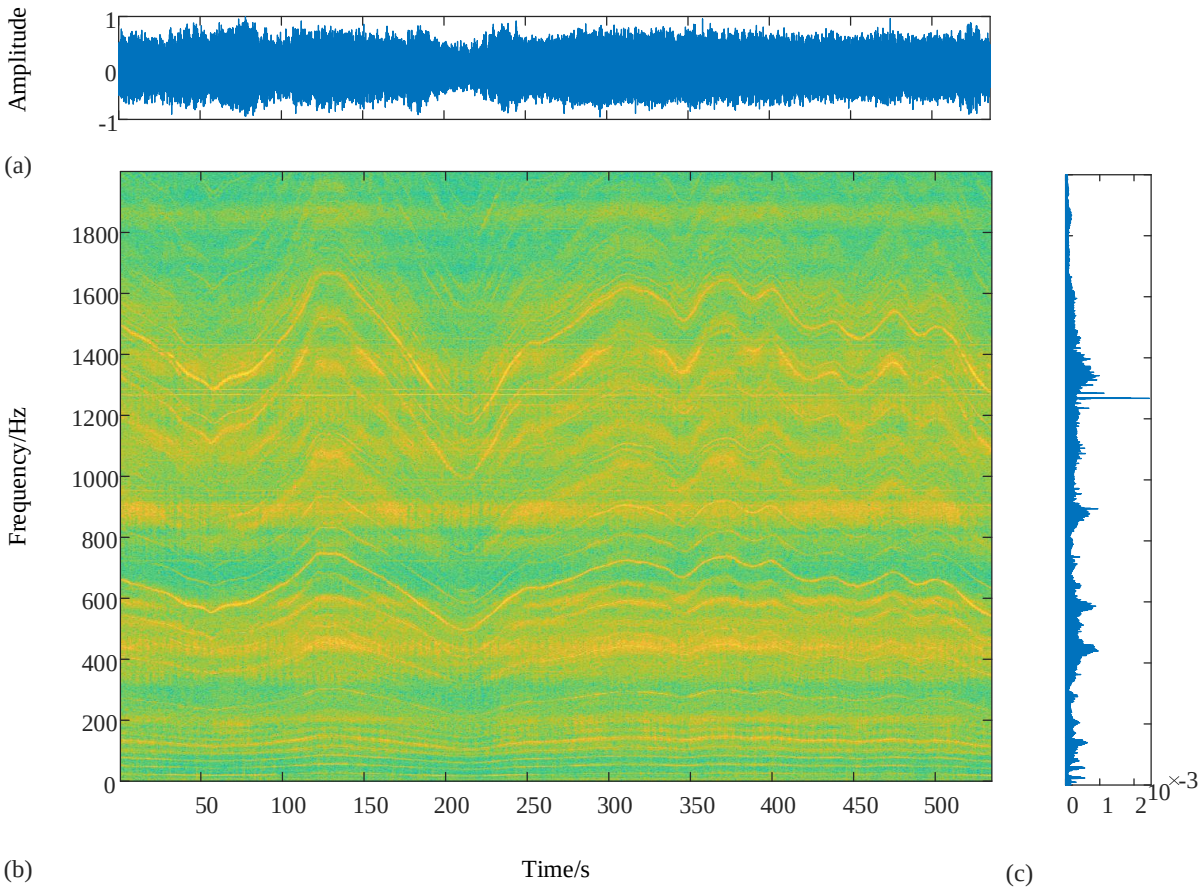


Figure 9: The (a) time plot and LSS's IAS, (b) spectrogram and (c) spectrum of the WT1 data.

To obtain an initial rough IAS estimate, the ridge of the first planetary GM harmonic is extracted from the signal spectrogram. Table 3 provides a comprehensive overview of the input parameters configured for different methods applied to the WT1 vibration signal. Two separate tests are conducted on the OIASAI using distinct order candidate sets: in the first test, the 2nd and 3rd planetary GM harmonics and the 1st intermediate GM harmonic are incorporated for IAS estimation refinement; in the second test, all potential harmonics are employed to evaluate the method's performance.

Table 3: Parameters used for IAS estimation of the WT1 signal

| Parameter | EIASAI | OIASAI -1 | OIASAI -2 | MHD |
|---|---|---|---|---|
| Fundamental harmonic/$h$ | 123, 637.71 | 123 | 123, 637.71 | 123, 637.71 |
| Sampling order/ $Os$ | 12300 | 12300 | 12300 | |

| | | | | |
|---|---|---|---|---|
| Used harmonics /$k$ | $h*\left\lfloor 1{:}\frac{Os}{2h}\right\rfloor$ | 246, 369 637.7 | $h*\left\lfloor 1{:}\frac{Os}{2h}\right\rfloor$ | $h*\left\lfloor 1{:}\frac{Os}{2h}\right\rfloor$ |
| Initial passband | $0.9k, 1.1k$ | $k-0.15\sqrt{k}, k+0.15\sqrt{k}$ | $k-0.15\sqrt{k}, k+0.15\sqrt{k}$ | 3 |

The IAS estimates derived from different methods, together with their corresponding estimation errors for the WT1 signal, are presented in Figure 10. OIASAI-2 yields the poorest estimation performance among all methods, as it treats all harmonics uniformly without differentiation. OIASAI-1 incorporates a subset of harmonics with the highest amplitudes for IAS estimation, thus achieving superior accuracy relative to OIASAI-2. Notably, EIASAI delivers the most accurate IAS estimates, with its time-varying estimation error remaining the smallest across the entire signal duration.

Figure 11 summarizes the MAE values and L1L2 norms of all methods across repeated iterations. Since OIASAI-2 treats all harmonics uniformly, its MAE increases continuously. In contrast, OIASAI-1 enhances estimation accuracy by carefully selecting shaft-synchronous harmonics as input components, with its performance quantified by a minimum MAE of 0.10%. Meanwhile, EIASAI and MHD achieve MAEs of 0.15% and 0.08%, respectively.

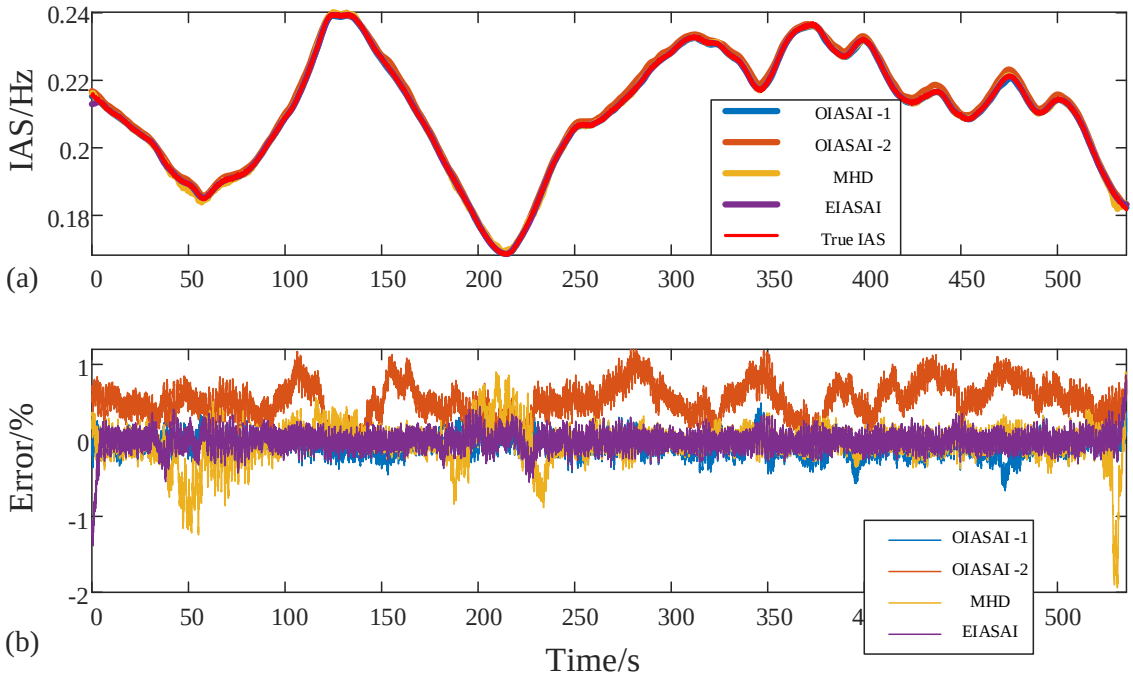


Figure 10 (a) Actual IAS and IAS estimated by different methods and (b) their corresponding error.

### 4.3 Wind turbine gearbox dataset 2

A second wind turbine dataset was sourced from two 2 MW units (designated as WT2 and WT3), both equipped with an identical gearbox configuration: a planetary gear stage with a fixed planet carrier serving as the input end, connected in series with two subsequent parallel gear stages (see Figure 12 for the configuration diagram). Vibration data were measured at the gearbox housing adjacent to the planetary gear stage. WT2 and WT3 provide signals with durations of 885s and 811s, respectively. Figures 13 and 14 display the time domain waveforms, frequency spectra and spectrograms of the two signals.

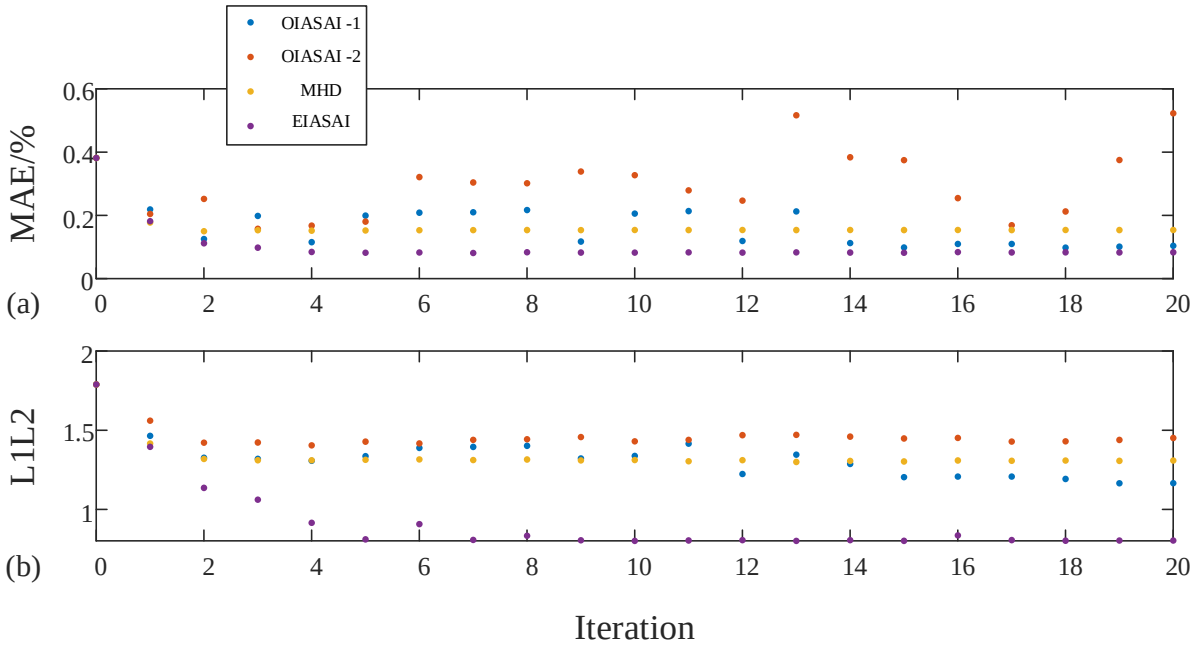


Figure 11 (a) MAE and (b) L1L2 of the estimated IAS in each iteration.

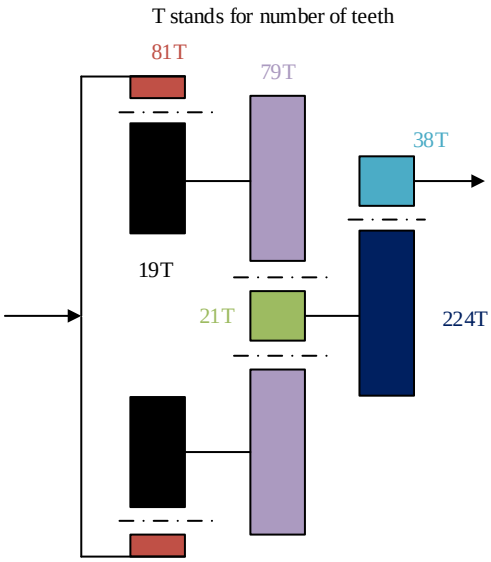


Figure 12: Kinematic configuration of the wind turbine dataset 2.

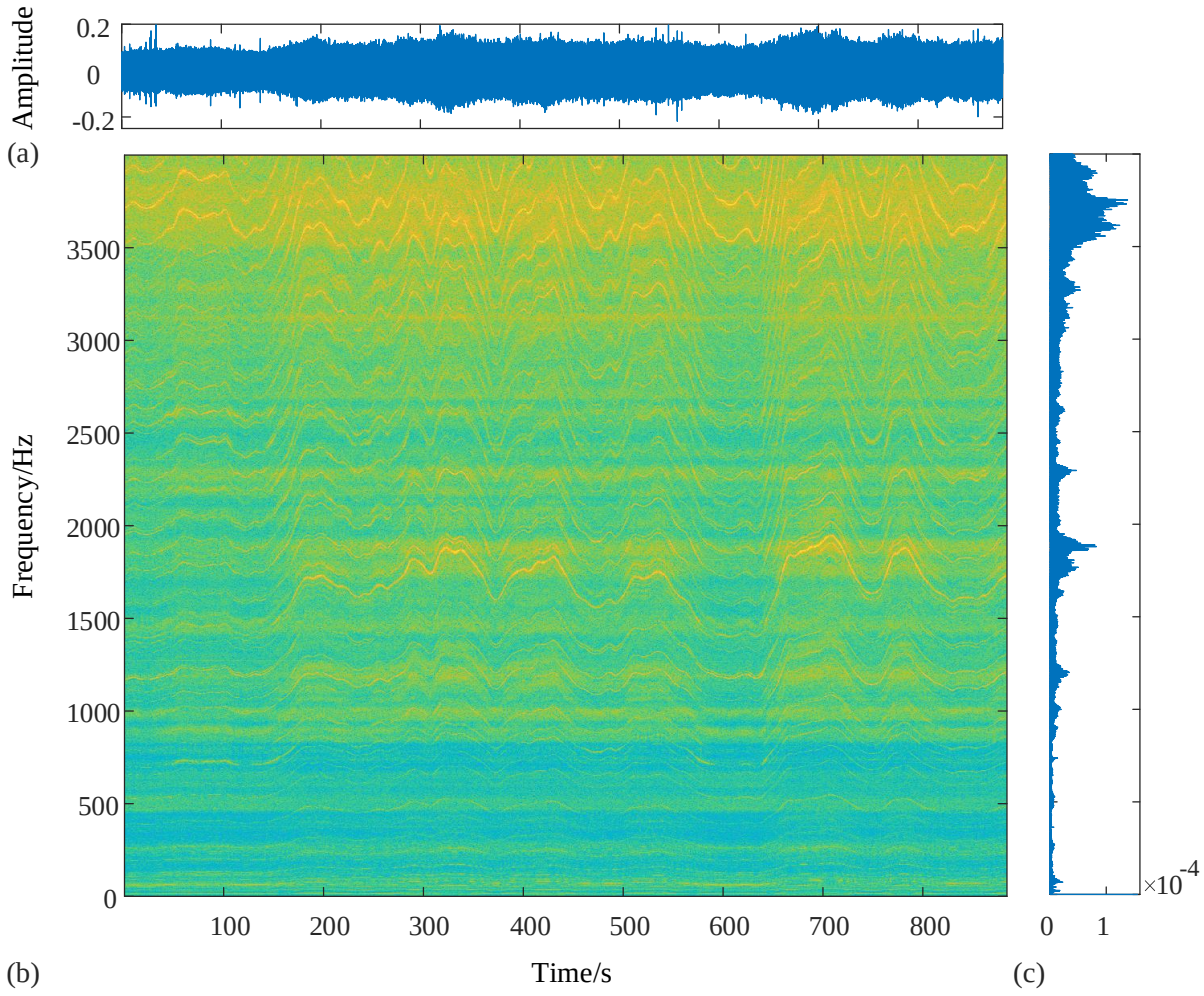


Figure 13. The (a) time plot, (b) spectrogram and (c) spectrum of the WT2 signal.

The ridge of the first intermediate GM harmonic is extracted to obtain a rough estimate of the IAS. A summary of the input parameters employed in this analysis is presented in Table 4. The OIASAI is further evaluated under two distinct harmonic candidate selection schemes: the first scheme selects the first two harmonics of all GM components, while the second scheme utilizes all available harmonics for IAS estimation.

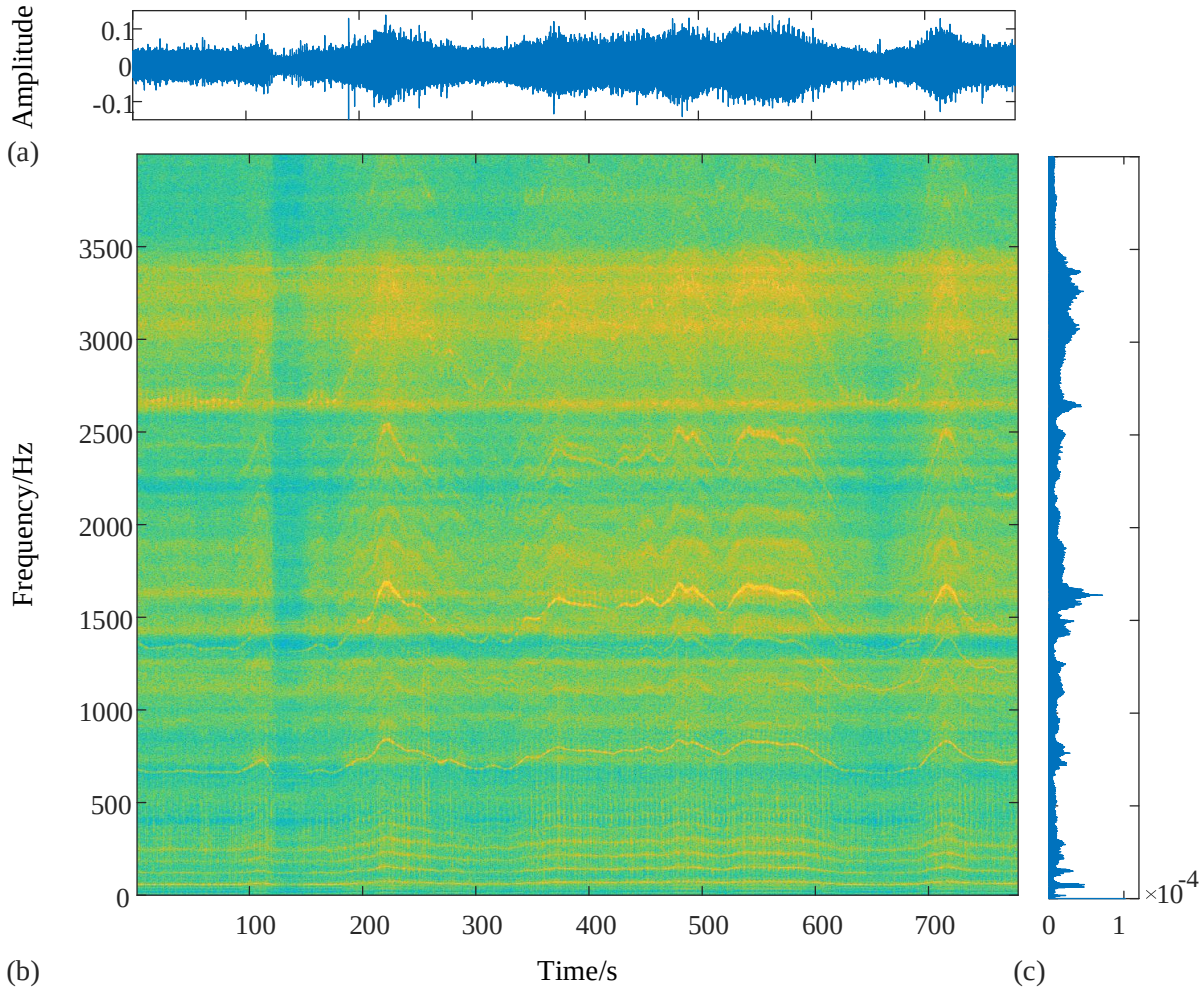


Figure 14. The (a) time plot, (b) spectrogram and (c) spectrum of the WT2 signal.

Table 4: Parameters used for IAS estimation of the WT2 and WT3 vibration signals

| Parameter | EIASAI | OIASAI -1 | OIASAI -2 | MHD |
|---|---|---|---|---|
| Fundamental harmonic/$h$ | 81, 336.79, 3592.42 | 81, 336.79 3592.42 | 81, 336.79, 3592.42 | 81, 336.793592.42 |
| Sampling order/ $Os$ | 30000 | 30000 | 30000 | |
| Used harmonics /$k$ | $h * \left\lfloor 1{:}\frac{Os}{2h} \right\rfloor$ | $h * [1{:}2]$ | $h * \left\lfloor 1{:}\frac{Os}{2h} \right\rfloor$ | $h * \left\lfloor 1{:}\frac{Os}{2h} \right\rfloor$ |

| | | | | |
|---|---|---|---|---|
| Initial passband | $0.9k, 1.1k$ | $k - 0.15\sqrt{k}, k + 0.15\sqrt{k}$ | $k - 0.15\sqrt{k}, k + 0.15\sqrt{k}$ | 3 |

Since the OIASAI-2 method once again exhibits excessive deviation from the true IAS (as shown in Figure 17), the IAS estimates derived from the other three methods—along with their corresponding estimation errors for the WT2 and WT3 signals—are presented in Figure 15. EIASAI yields the most accurate results for both cases. Consistent findings are illustrated in Figure 16, which summarizes the MAE and L1L2 values for all IAS estimation methods. OIASAI-1, MHD, and EIASAI all converge within 5 iterations and yield improved IAS estimation accuracy, with corresponding MAEs of 0.10%, 0.19%, and 0.08% for the WT2 signal and 0.11%, 0.22%, and 0.08% for the WT3 signal, respectively

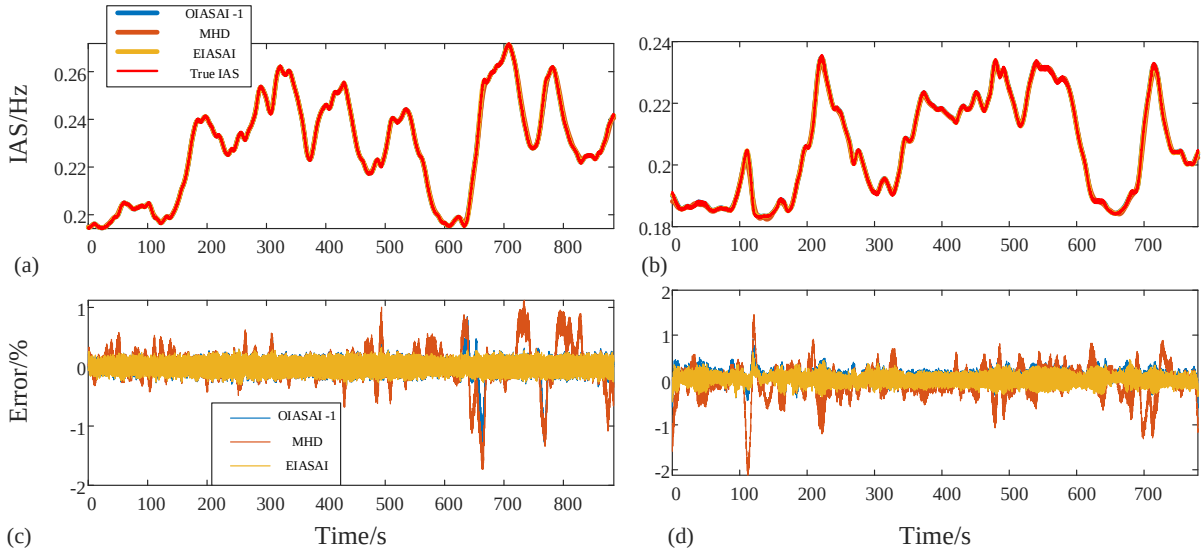


Figure 15 (a) and (b) Actual IAS and IAS estimated by different methods and (c) and (d) their corresponding error; (left) WT2 signal and (right) WT3 signal.

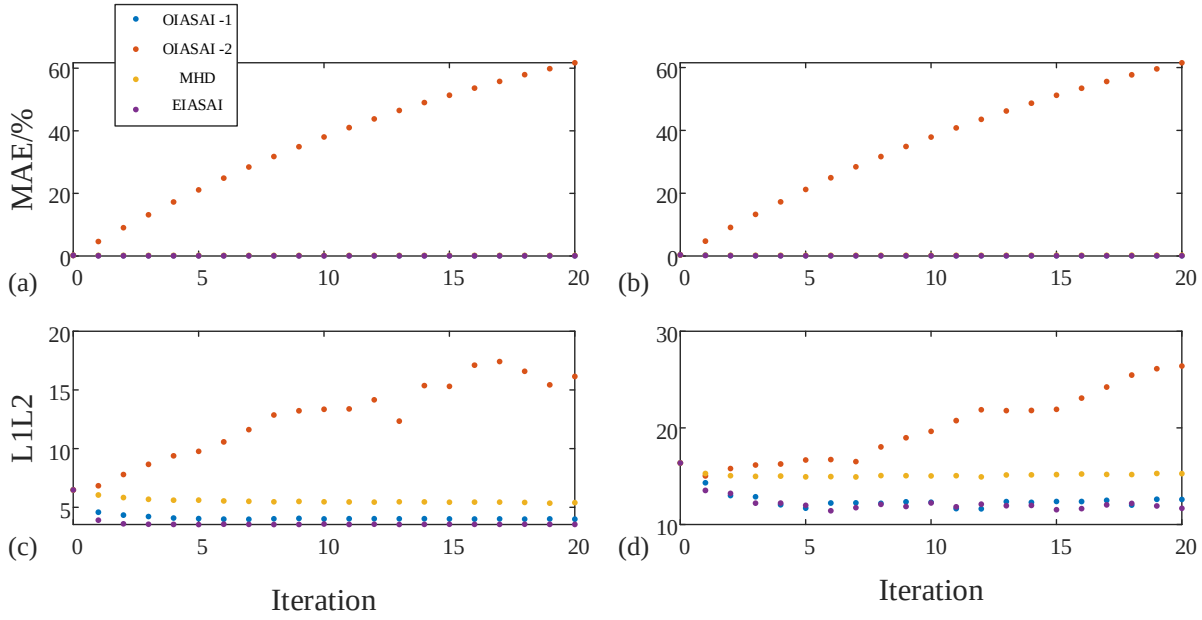


Figure 16 (a) and (b) MAE and (c) and (d) L1L2 of the estimated IAS in each iteration; (left) WT2 signal and (right) WT3 signal.

## 5. Conclusions

Amid the rapid expansion of the wind energy sector in recent years, tacholess order tracking has garnered increasing attention. IAS estimation based on phase demodulation represents one of the most pivotal techniques in this field. In this study, the interactive effects of carrier signal amplitude, amplitude modulation, and background noise on IAS estimation performance are comprehensively investigated. It is demonstrated that the fluctuation of IAS is dependent on these three key factors. On the basis of this insight, an enhanced IAS accuracy refinement method (EIASAI) is proposed, which incorporates both IAS estimates derived from all harmonic components and their corresponding variance estimates. Compared with the original IAS accuracy improvement method, the proposed EIASAI approach reduces reliance on expert experience in harmonic selection, thereby rendering it more suitable for practical industrial applications. The robustness of the proposed method was validated through both numerical simulations and real-world wind turbine datasets.

## Acknowledgement

This work is supported by the National Natural Science Foundation of China (52105134).

# Appendices

## A. Variance Derivation for 1st-Order Difference of Band-Limited White Noise Orthogonal Component

Let $w_\perp(n)$ be a discrete-time signal. Its first-order difference is defined as:

$$\Delta w_\perp(n) = w_\perp(n) - w_\perp(n-1) \tag{A.1}$$

Using the variance property $\mathrm{Var}[X-Y] = \mathrm{Var}[X] + \mathrm{Var}[Y] - 2\mathrm{Cov}[X,Y]$, the variance of $\Delta w_\perp(n)$ is:

$$\begin{aligned}\mathrm{Var}[\Delta w_\perp(n)] &= \mathrm{Var}[w_\perp(n) - w_\perp(n-1)] \\ &= \mathrm{Var}[w_\perp(n)] + \mathrm{Var}[w_\perp(n-1)] - 2\mathrm{Cov}[w_\perp(n), w_\perp(n-1)]\end{aligned} \tag{A.2}$$

For a band-limited white signal where mean and variance is nearly time-invariant:

$$\mathrm{Var}[w_\perp(n)] \approx \mathrm{Var}[w_\perp(n-1)] \approx \mathrm{Var}[w_\perp] \tag{A.3}$$

The 1st-order autocorrelation coefficient $\rho_{w_\perp}(1)$ of $w_1(n)$ is defined as:

$$\rho_{w_\perp}(1) = \frac{\mathrm{Cov}[w_\perp(n), w_\perp(n-1)]}{\mathrm{Var}[w_\perp]} \tag{A.4}$$

Rearranging gives $\mathrm{Cov}[w_\perp(n), w_\perp(n-1)] = \rho_{w_\perp}(1) \cdot \mathrm{Var}[w_\perp]$

Substitute the above results into the variance expression:

$$\begin{aligned}\mathrm{Var}[\Delta w_\perp(n)] &= \mathrm{Var}[w_\perp] + \mathrm{Var}[w_\perp] - 2 \cdot \rho_{w_\perp}(1) \cdot \mathrm{Var}[w_\perp] \\ &= 2\mathrm{Var}[w_\perp] \cdot \left[1 - \rho_{w_\perp}(1)\right]\end{aligned} \tag{A.5}$$

## B. Single realization based approach for 1st-Order Difference of Band-Limited White Noise Orthogonal Component

Consider the orthogonal component $w_\perp(n)$ (a baseband signal with bandwidth $B = f_2 - f_1$) of band-limited white noise. Its PSD is:

$$S_{\Delta w_\perp(n)}(f) = \begin{cases} N_0, & |f| < B/2 \\ 0, & \text{otherwise} \end{cases} \tag{B.1}$$

The PSD of the differenced signal $\Delta w_\perp(n)$ is:

$$S_{\Delta w_1}(f) = 4\sin^2\left(\pi \frac{f}{f_s}\right) \cdot S_{w_1}(f) \tag{B.2}$$

By the Wiener-Khinchin theorem, the variance of the differenced orthogonal component is:

$$\mathrm{Var}[\Delta w_{\perp}(n)] = \int_{-B/2}^{B/2} S_{\Delta w_1}(f)df = 4\int_{-B/2}^{B/2} \sin^2\left(\pi\frac{f}{f_s}\right)\cdot N_0 df \tag{B.3}$$

When the center frequency $f_c$ of the bandpass filter satisfies $f_c \gg B$, $f \approx f_c$ holds within the bandwidth. Thus, $\sin^2(\pi f T_s) \approx \sin^2\left(\pi\frac{f}{f_s}\right)$, and the integral simplifies to:

$$\mathrm{Var}[\Delta w_{\perp}(n)] = 4N_0\sin^2\left(\pi\frac{f_c}{f_s}\right)\cdot B \tag{B.4}$$

Note that $N_0 B = \sigma^2$ (the variance of the orthogonal component of band-limited white noise). Substituting this into the equation yields the final approximate variance:

$$\mathrm{Var}[\Delta w_{\perp}(n)] = 4\sigma^2\sin^2\left(\pi\frac{f_c}{f_s}\right) \tag{B.5}$$

## References


[1] D. Rémond, J. Antoni, R.B. Randall, Editorial for the special issue on Instantaneous Angular Speed (IAS) processing and angular applications, Mech. Syst. Signal Process. 44 (2014) 1–4.

[2] J. Urbanek, T. Barszcz, J. Antoni, A two-step procedure for estimation of instantaneous rotational speed with large fluctuations, Mech. Syst. Signal Process. 38 (2013) 96–102. https://www.sciencedirect.com/science/article/pii/S0888327012002270 (accessed September 19, 2019).

[3] F. Bonnardot, M. El Badaoui, R.B. Randall, J. Danière, F. Guillet, Use of the acceleration signal of a gearbox in order to perform angular resampling (with limited speed fluctuation), Mech. Syst. Signal Process. 19 (2005) 766–785.

[4] M. Zhao, J. Lin, X. Wang, Y. Lei, J. Cao, A tacho-less order tracking technique for large speed variations, Mech. Syst. Signal Process. 40 (2013) 76–90.

[5] F. Combet, R. Zimroz, A new method for the estimation of the instantaneous speed relative fluctuation in a vibration signal based on the short time scale transform, Mech. Syst. Signal Process. 23 (2009) 1382–1397.

[6] F. Millioz, N. Martin, Time-Frequency Segmentation for Engine Speed Monitoring, Thirteen. Int. Congr. Sound Vib. (2006).

[7] S. Schmidt, P.S. Heyns, J.P. de Villiers, A tacholess order tracking methodology based on a probabilistic approach to incorporate angular acceleration information into the maxima

tracking process, Mech. Syst. Signal Process. 100 (2018) 630–646.

[8] R. Zimroz, J. Urbanek, T. Barszcz, W. Bartelmus, F. Millioz, N. Martin, Measurement of instantaneous shaft speed by advanced vibration signal processing - Application to wind turbine gearbox, Metrol. Meas. Syst. 18 (2011) 701–712.

[9] Q. Leclère, H. André, J. Antoni, A multi-order probabilistic approach for Instantaneous Angular Speed tracking debriefing of the CMMNO14′ diagnosis contest, Mech. Syst. Signal Process. 81 (2016) 375–386.

[10] Y. Li, X. Zhang, Z. Chen, Y. Yang, C. Geng, M.J. Zuo, Time-frequency ridge estimation : An effective tool for gear and bearing fault diagnosis at time-varying speeds, Mech. Syst. Signal Process. 189 (2023) 110108.

[11] J. Yoo, J. Park, T. Kim, J. Moon Ha, B.D. Youn, Weighted multi-order Viterbi algorithm (WMOVA): Instantaneous angular speed estimation under harsh conditions, Mech. Syst. Signal Process. 211 (2024).

[12] F. Karkafi, Q. Leclère, J. Antoni, D. Abboud, A multi-order synchrosqueezing transform leveraging informative harmonics selection for instantaneous angular speed estimation, Mech. Syst. Signal Process. 230 (2025) 112567.

[13] M. Feldman, Hilbert transform in vibration analysis, Mech. Syst. Signal Process. 25 (2011) 735–802.

[14] R.B. Randall, W.A. Smith, Uses and mis-uses of energy operators for machine diagnostics, Mech. Syst. Signal Process. 133 (2019) 106199.

[15] M.D. Coats, R.B. Randall, Single and multi-stage phase demodulation based order-tracking, Mech. Syst. Signal Process. 44 (2014) 86–117.

[16] D. Peng, W.A. Smith, R.B. Randall, Z. Peng, C.K. Mechefske, Speed estimation in planetary gearboxes a method for reducing impulsive noise, Mech. Syst. Signal Process. (n.d.).

[17] D. Peng, Y. Chen, M.J. Zuo, C.K. Mechefske, Assessment and improvement of the accuracy of tacholess instantaneous speed estimation, Mech. Syst. Signal Process. 202 (2023).

[18] D. Peng, W.A. Smith, R.B. Randall, K. Feng, Z. Peng, W. Teng, Y. Liu, Iterative improvement in tacholess speed estimation using instantaneous error estimation for machine

condition monitoring in variable speed, Mech. Syst. Signal Process. 216 (2024) 111488.

[19] C. Peeters, J. Antoni, Q. Leclère, T. Verstraeten, J. Helsen, Multi-harmonic phase demodulation method for instantaneous angular speed estimation using harmonic weighting, Mech. Syst. Signal Process. 167 (2022).

[20] C.M. Spooner, Multi-resolution white-space detection for cognitive radio, in: IEEE Mil. Commun. Conf., 2007.

[21] C. Peeters, Q. Leclère, J. Antoni, P. Lindahl, J. Donnal, S. Leeb, J. Helsen, Review and comparison of tacholess instantaneous speed estimation methods on experimental vibration data, Mech. Syst. Signal Process. 129 (2019) 407–436.